Smart Structures and Systems, *Vol. 12, No. 2 (2013) 097-119*
DOI:http://dx.doi.org/10.12989/sss.2013.12.2.097

Predictive model of fatigue crack detection in thick bridge steel structures with piezoelectric wafer active sensors

M. Gresil*, L. Yu , Y. Shen and V. Giurgiutiu

University of South Carolina, Department of Mechanical Engineering, 300 Main Street, Columbia, SC, 29201, USA

(Received March 20, 2012, Revised July 27, 2012, Accepted October 27, 2012)

Abstract. This paper presents numerical and experimental results on the use of guided waves for structural health monitoring (SHM) of crack growth during a fatigue test in a thick steel plate used for civil engineering application. Numerical simulation, analytical modeling, and experimental tests are used to prove that piezoelectric wafer active sensor (PWAS) can perform active SHM using guided wave pitch-catch method and passive SHM using acoustic emission (AE). AE simulation was performed with the multi-physic FEM (MP-FEM) approach. The MP-FEM approach permits that the output variables to be expressed directly in electric terms while the two-ways electromechanical conversion is done internally in the MP-FEM formulation. The AE event was simulated as a pulse of defined duration and amplitude. The electrical signal measured at a PWAS receiver was simulated. Experimental tests were performed with PWAS transducers acting as passive receivers of AE signals. An AE source was simulated using 0.5-mm pencil lead breaks. The PWAS transducers were able to pick up AE signal with good strength. Subsequently, PWAS transducers and traditional AE transducer were applied to a 12.7-mm CT specimen subjected to accelerated fatigue testing. Active sensing in pitch catch mode on the CT specimen was applied between the PWAS transducers pairs. Damage indexes were calculated and correlated with actual crack growth. The paper finishes with conclusions and suggestions for further work.

Keywords: acoustic emission; active sensing; finite element method; crack detection; piezoelectric wafer active sensor; structural health monitoring; predictive modeling

1. Introduction

The current stage of bridges in the United States calls for the implementation of a continuous bridge monitoring system that can aid in timely detection of damage and help extend the service life of these structures. A typical monitoring system would be one that enables non-invasive continuous monitoring of the structure. Structural health monitoring (SHM) is an emerging technology that can be used to identify, locate, and quantify damage in a structural member or system before failure occurs. Passive SHM monitors acoustic emission (AE) that arrives as guided waves generated by the crack opening in thin wall structures. AE occurs due to stress waves generated when there is a rapid release of energy in a material during a fatigue crack test. Active SHM systems using interrogative Lamb waves are able to cover large areas from a single location

*Corresponding author, Post-doctoral Research Fellow, E-mail: matthieu@mailbox.sc.edu

http://www.techno-press.org/?journal=sss&subpage=8 ISSN: 1738-1584 (Print), 1738-1991 (Online)

making such systems cost effective and efficient. Another advantage is that high frequency Lamb waves also provide through-the-thickness interrogation which allows detection of internal defects in materials. Piezoelectric wafer active sensors (PWAS) have been used for both active and passive SHM.

Lamb wave signals are difficult to characterize because of the complex nature of the signals due to the multimodal character of the Lamb waves. Work has been done to establish analytically the dispersion curves (Lamb 1917, Viktorov 1967, Achenbach 1973, Harker 1987, Dieulesaint and Royer 1996, Rose 1999), to validate experimentally (Grondel *et al.* 1999) and to study the effect of dispersion over long distances (Wilcox *et al.* 2001). The phenomena of interaction between the ultrasonic wave and the defect and/or the structure, leading to a complex signature (reflection, diffraction, mode conversion, etc.) must be simulated to compare with a specific response signal actually received by a sensor. Many authors have already investigated the interaction of Lamb modes with a single defect like crack, notch or circular cavity. Some of them used analytical (Grahn 2003) or semi-analytical (Castaings 2002) solutions. Whereas other authors (Dietzhausen *et al.* 1998, Moder and Jacobs 1998, Zak *et al.* 2006, Lee *et al.* 2006, Han 2007, Liu and Giurgiutiu 2007, Greve *et al.* 2008, Lu *et al.* 2008, Yang and Hu 2008, Wang *et al.* 2008, Gresil *et al.* 2011a, Gresil *et al.* 2011b, Giurgiutiu *et al.* 2012, Gresil *et al.* 2012) chose the finite element method (FEM) to simulate the elastic wave propagation associated with acoustic phenomena and ultrasounds problems.

In this paper, we present the work on multi-physics based FEM modeling of (1) PWAS transducers using piezoelectric element and (2) the plate using a mechanical element. This approach is also used to simulate the AE received by the PWAS. To validate the FEM approach, analytical wave propagation is developed as well. Both are compared with the experimental results. Our general approach is to first use passive AE-SHM system to detect crack propagation and then use the active SHM system (i.e., ultrasonic pitch-catch method) to quantify the growth of the crack. The originality of this approach is in using the same sensor, the PWAS, for both passive and active SHM sensing.

2. State of the ART

2.1 Acoustic emission from cracking

Acoustic emission (AE) is a passive SHM technique that can be used for many applications. When crack grows, energy is released at the crack tip in form of waves. AE sensors can be used to measure these waves. Several sensors in combination can be used to estimate the severity of the crack and its location. Most publications show results from fatigue cracks in bulk materials and qualitative results from real structures (Scruby *et al.* 1985). However, there is limited literature presenting quantitative results from plate-like structures and a lot of the experiments are based on simulated AE sources, e.g., pencil lead breaks (Gorman and Prosser 1991). One aim of this paper is to analyze the elastic waves generated from fatigue cracks in a thick isotropic structure for the civil engineering application. FEM can be used to model the AE waves from fatigue crack (Hill *et al.* 2004) and it can provide a better understanding of the AE generated from fatigue cracks in plates).

2.2 Active SHM

Active SHM is concerned directly with assessing the state of the structural health by trying to detect the presence and extent of structural damage. In this respect, active SHM approach is similar with the approach taken by non-destructive evaluation (NDE) methodologies, only that active SHM takes it one step further: active SHM attempts to develop damage detection sensors that can be permanently installed on the structure and monitoring methods that can provided on demand structural health bulletins (Giurgiutiu 2008). An active monitoring system can also reduce the duration of inspection, and, as opposed to passive detection systems, it does not require continue monitoring.

2.3 Guided waves

Guided waves are very widespread in SHM applications: Guided waves are important for SHM applications because they have the particularity to travel without much energy loss over large structured areas. These properties make them well suited for ultrasonic inspection of bridge, aircraft, ships, missiles, pressure vessels, pipelines, etc. In plates, ultrasonic guided waves propagate as Lamb waves and as shear horizontal waves (SH). Ultrasonic guided waves in plates were first described by Lamb (1917). A detailed study of Lamb waves has been given by Viktorov (1967), Achenbach (1973), Graff (1975), Rose (1999) and Dieulesaint and Royer (1996). Lamb waves are of two varieties, symmetric modes (S0, S1, S2...) and anti-symmetric modes (A0, A1, A2...). At low values of the frequency-thickness product, fd ,the first symmetric mode, S0, resembles axial waves whereas the first anti-symmetric mode, A0, resembles flexural waves. The choice of Lamb waves is justified by their many advantages; they have the power to energize the entire thickness of the plate and offer the possibility of detecting internal defects at various depths. However, Lamb waves present some difficulties: they are dispersive, and also several modes can propagate at different speeds at a given frequency. Work has been done to establish analytically the dispersion curves (Harker 1987, Dieulesaint and Royer 1996), to validate the results experimentally and to study the effect of dispersion over long distances (Wilcox *et al.* 2001). Lamb wave propagation was used by many authors (Alleyne and Cawley 1992, Mal and Chang 1999, Lemistre and Balageas 2001) using piezoelectric disks as transmitters and receivers to measure the changes in the signal received from a structure having a defect. This method has proved good efficiency for detection of cracks, holes, corrosion in metallic materials. However the signal processing is complex due to multiple reflections. Today the majority of work concerns the propagation of Lamb waves in thin structures. Regarding the interaction of Lamb waves with different types of damage, many experimental studies are: detection of impact (Frankenstein *et al.* 2006), cracks (Grondel *et al.* 2002) or corrosion (Titry *et al.* 2004). For this reason it is very important to study the Lamb wave propagation in thick steel plates to understand the difficulties in analyzing these waves.

3. Analytical modeling

The analytical modeling is carried out in frequency domain, and could be described by four steps: (i) The excitation signal $V_e(t)$ is Fourier transformed into $V_e(\omega)$; (ii) the plate transfer function in frequency domain is obtained as $G(\omega)$; (iii) the excitation signal and the plate transfer function are multiplied to obtain the receiver signal in frequency domain $V_r(\omega) = V_e(\omega) \cdot G(\omega)$; (iv)

the receiver signal is inverse Fourier transformed back into time domain and the waveform in time domain is obtained as $V_r(t) = IFFT\{V_r(\omega)\} = IFFT\{V_e(\omega)\cdot G(\omega)\}$, where IFFT denotes inverse Fourier transform and $G(\omega)$ is the frequency-dependent structure transfer function that affects the wave propagation through the medium. In this paper, the main interest is on symmetric fundamental Lamb wave mode (S0) and anti-symmetric fundamental Lamb wave mode (A0). This approach is a 2D plane strain problem and the PWAS transducer is simplified as surface force loading. For Lamb waves with only two modes (A0 and S0) excited, the structure transfer function $G(\omega)$ can be expressed as (Giurgiutiu 2008)

$$\begin{aligned}\varepsilon_x(x,t)\Big|_{y=d} = &-i\frac{a\tau_0}{\mu}(\sin k^S a)\frac{N_S\left(k^S\right)}{D_S^{'}\left(k^S\right)}e^{-i\left(k^S x-\omega t\right)}\\ &-i\frac{a\tau_0}{\mu}(\sin k^A a)\frac{N_A\left(k^A\right)}{D_A^{'}\left(k^A\right)}e^{-i\left(k^A x-\omega t\right)}\end{aligned} \tag{1}$$

So, $G(\omega)$ can be written as

$$G(\omega) = S(\omega)e^{-ik^S x} + A(\omega)e^{-ik^A x} \tag{2}$$

With

$$\begin{aligned}S(\omega) &= -i\frac{a\tau_0}{\mu}(\sin k^S a)\frac{N_S\left(k^S\right)}{D_S^{'}\left(k^S\right)}\\ A(\omega) &= -i\frac{a\tau_0}{\mu}(\sin k^A a)\frac{N_A\left(k^A\right)}{D_A^{'}\left(k^A\right)}\end{aligned} \tag{3}$$

$$D_S = \left(k^2-\beta^2\right)^2\cos(\alpha d)\sin(\beta d) + 4k^2\alpha\beta\sin(\alpha d)\cos(\beta d) \tag{4}$$

$$D_A = \left(k^2-\beta^2\right)^2\sin(\alpha d)\cos(\beta d) + 4k^2\alpha\beta\cos(\alpha d)\sin(\beta d) \tag{5}$$

$$N_S = k\beta\left(k^2-\beta^2\right)\cos(\alpha d)\sin(\beta d) \qquad N_A = k\beta\left(k^2-\beta^2\right)\sin(\alpha d)\cos(\beta d) \tag{6}$$

$$\begin{aligned}\alpha^2 &= \frac{\omega^2}{c_p^2} - k^2\\ \beta^2 &= \frac{\omega^2}{c_s^2} - k^2\end{aligned} \tag{7}$$

where a is the half length of the PWAS, $2d$ is the plate thickness , τ_0 is the shear stress between PWAS and the plate, μ is shear modulus, k^S and k^A are the wavenumbers for S_0 and A_0 respectively, x denotes the distance between the two PWAS transducers, and c_p and c_s are the wave speed for

pressure wave and shear wave. In the transfer function $G(\omega)$, the functions $S(\omega)$ and A(ω) determine the amplitude of S0 and A0 modes. The terms $\sin(k^S a)$ and $\sin(k^A a)$, in $S(\omega)$ and $A(\omega)$ control the wave mode tuning effect.

The wave speed dispersion curve is obtained by solving Rayleigh-Lamb equations, which are transcendental equations that require numerical solution. The usual form of Rayleigh Lamb equations are as follows

$$\frac{\tan(\beta d)}{\tan(\alpha d)} = -\frac{4\alpha\beta k^2}{\left(k^2-\beta^2\right)^2} \qquad \frac{\tan(\beta d)}{\tan(\alpha d)} = -\frac{\left(k^2-\beta^2\right)^2}{4\alpha\beta k^2} \tag{8}$$

After getting the wave speed dispersion curve, the wavenumber for each frequency component i.e., $k = \omega/c$ is known. Thus, all the terms involved in the plate transfer function could be solved, and the plate transfer function $G(\omega)$ is obtained. After the plate transfer function $G(\omega)$ is obtained, the excitation signal is Fourier transformed.

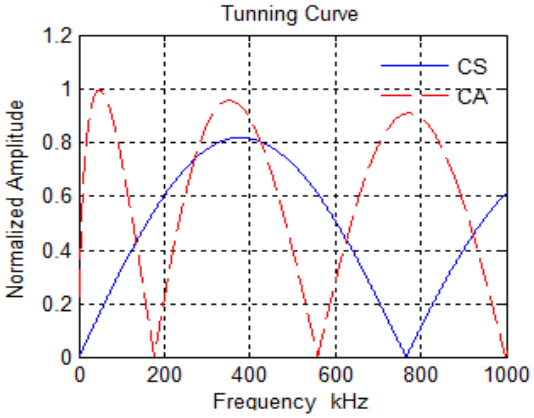

Fig. 1 Amplifying coefficients C_S and C_A versus the frequency for a 1D plate of 1-mm thick and a PWAS dimension of 7-mm

4. Finite element modeling

4.1 2D FEM modeling of guided wave propagation

A theoretical solution for the magnitude of frequency contents of S0 and A0 wave packets could be derived from Eqs. (4) and (5) after discarding the factor which does not influence amplitude relation

$$\left|V_{Sr}(\omega)\right| = \left|\left(\sin k^S a\right)\frac{N_S\left(k^S\right)}{D_S'\left(k^S\right)}\right| \qquad \left|V_{Ar}(\omega)\right| = \left|\left(\sin k^A a\right)\frac{N_A\left(k^A\right)}{D_A'\left(k^A\right)}\right|\left|V_e(\omega)\right| \tag{9}$$

So, the amplification coefficients for each package are

$$C_S = \left| \left(\sin k^S a \right) \frac{N_S\left(k^S\right)}{D_S'\left(k^S\right)} \right| \qquad C_A = \left| \left(\sin k^A a \right) \frac{N_A\left(k^A\right)}{D_A'\left(k^A\right)} \right| \tag{10}$$

The amplification coefficients are directly related to the PWAS size *a*, material properties, plate thickness and the corresponding frequency.

The Fig. 1 represents the amplifying coefficients C_S and C_A versus the frequency. We can observe that these curves are very similar to the tuning curve discussed by Giurgiutiu (2005) and Santonai-Bottai *et al.* (2007).

A theoretical solution is obtained for a 150 kHz Hanning window modulated sine tone burst excitation signal by a 7-mm PWAS transducer coupling with a 1-mm thick Aluminum plate. The frequency contents of A0 and S0 pitch-catch signals are shown in Fig. 2. When modeling by finite element and analytical model simulates the PWAS transducer by a single point force, i.e., $a \to 0$, the frequency shift becomes zero.

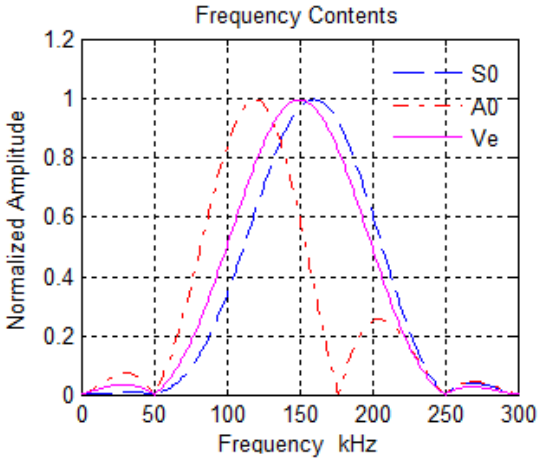

Fig. 2 Frequency contents of S0 and A0 packets and excitation Ve at 150 kHz

In the context of wave propagation FEM modeling, the choice of the solving technique, mesh density and time step influences the successful outcomes of the exercise but also the level of accuracy with which the phenomenon is represented. For time domain models solved with an explicit solver, we investigate the influence of the mesh density for linear quadrilateral elements for both A0 and S0 modes waves using the commercial software ABAQUS. Both S0 and A0 wave generations excited by a pair of self-equilibrating nodal forces are considered. The distance between the nodes where the two forces are applied corresponds to the PWAS size. The time domain excitation signal considered in our studies consisted of a 150 kHz three-count tone burst modulated through a Hanning window. The distance between the transducer and the receiver is 100 mm. The mesh density is expressed as $N = \lambda / L$ in terms of elements per wavelength, where λ is the wavelength and L is the size of the FEM element. Fig. 3 highlights the strong influence of

the mesh density on the group velocity error for the A_0 mode. The curve shows how the error varies from a value of about 9% for $N=15$ to a value of 0.2% for $N=254$. For the fundamental symmetric mode S_0, the error varies from a value of about 2% for $N=20$ to a value of 0.15% for $N=120$.

As mentioned previously, the mesh density value has a great impact on the computational model size and therefore the amount of memory required solving the model.

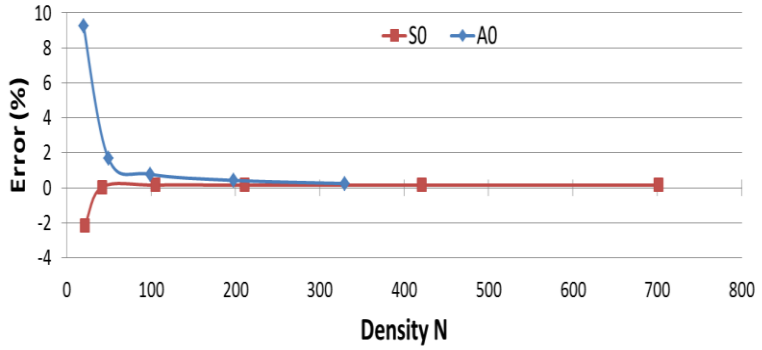

Fig. 3 Group velocity error versus the mesh density for the S0 and A0 modes

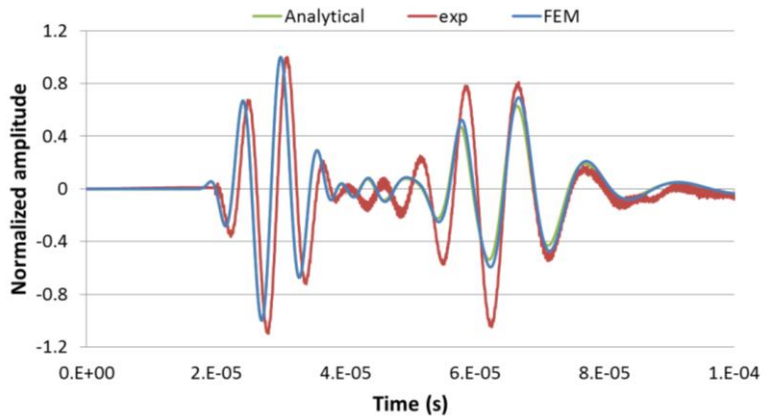

Fig. 4 Comparison between the analytical, the FEM and the experimental receive signal from the PWAS at 150 kHz

A comparison of the analytical modeling, the finite element modeling, and the experimental results for a 1-mm thick aluminum plate with 100-mm PWAS distance for a frequency of 150 kHz is shown in Fig. 4. S0 and A0 mode wave packages can be observed. The wave speed of S0 mode is higher than the A0 mode, so the S0 wave packet is picked up earlier than the A0 wave packet. Since the excitation signal has a center frequency of 150 kHz, we would have thought that the center frequencies of the S0 and A0 wave packets are also 150 kHz. In fact, as shown in Fig. 5,

this is not the case. We note that the center frequency of the A0 packet undergone a shift towards lower frequencies while the S0 packet undergone a shift towards higher frequencies. This phenomenon is due to the tuning curves and the amplification coefficients as explained in the Eq. (10) and the Fig. 4.

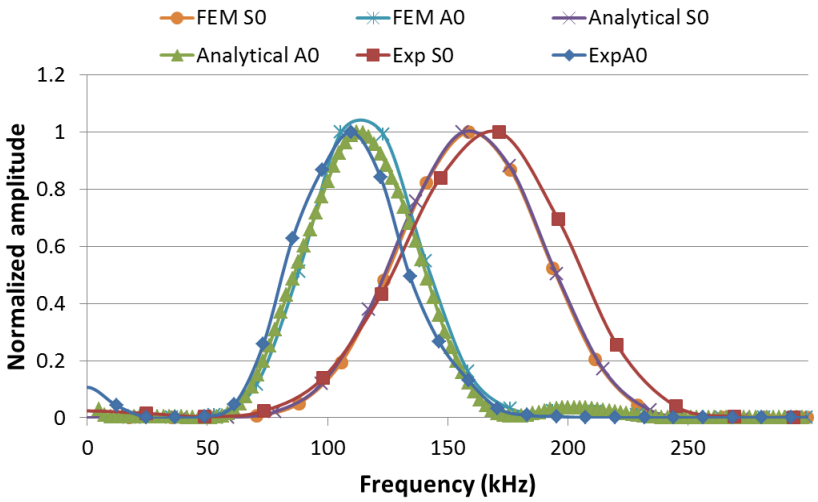

Fig. 5 FFT of the S0 wave packet and the A0 mode packet for the analytical, FEM and experimental signal received

4.2 3D FEM modeling of guided wave propagation

In SHM applications, the fundamental anti-symmetrical mode (A0) is often preferable and more sensitive to damage because its wavelength is shorter than that of the S0 mode at a given frequency.

However, the A0 mode exhibits more dispersion at low frequencies. The FEM simulation of the A0 mode requires fine spatial discretization with substantial computational cost because of the short wavelength. In contrast, the mode shapes of the S0 mode are simpler and the stresses are almost uniform throughout the thickness of the plate at low values to the frequency-plate thickness product (Lowe and Diligent 2002). For these reasons, both the S0 and A0 modes were selected in this study to evaluate the interaction of Lamb waves with a hole.

We modeled the guided wave generation and reception with a PWAS network in a rectangular 12.7-mm thick steel plate containing a through-hole defect (Fig. 6(a)). We used the ABAQUS/explicit solver because it gives a better trade-off between accuracy and computation time. The piezoelectric element does not exist in ABAQUS/explicit; hence we applied 12 self-equilibrating forces as shown in Fig. 6(b) to simulate the wave excitation.

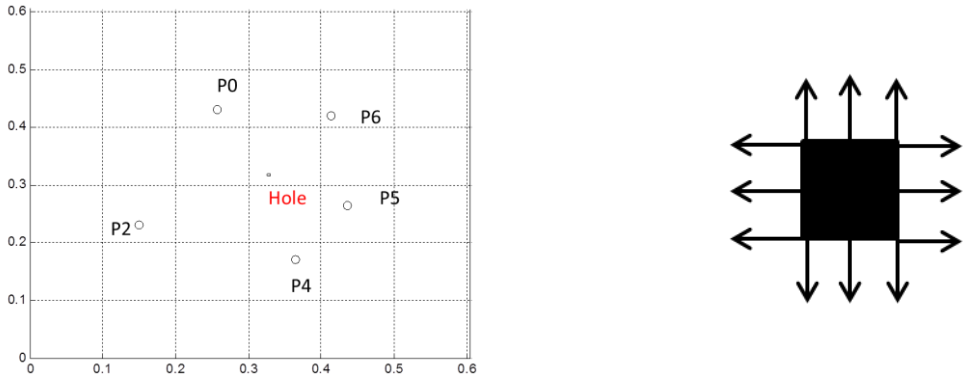

Fig. 6 (a) FEM and experimental configuration of a thick 12-mm steel plate and (b) self-equilibrated forces applied to simulate the displacement occur by the PWAS P0

A 3-count smoothed tone burst with a central frequency of 141 kHz was used to modulate the excitation. (This frequency corresponds of the best experimental damage detection configuration for this type of defect and plate thickness). The excitation was applied to PWAS P0 and received by PWAS P4 (Fig. 6(a)). The wave reception was modeled by monitoring the radially resolved surface strain ε_r at the center of the receiver PWAS. Fig. 7 shows the analytical and FEM simulations compared with experimental measurement at PWAS P4. The first wave packet corresponds to the S0 mode. A very good agreement is observed between the experimental and the FEM results. The analytical solution is not as good; this may be due to the fact that the analytical model is only a 1D model. The second wave packet corresponds to the A0 mode. Here, we observe a very good agreement between the analytical results and the FEM results. But we observe a time shift between these two results and the experimental result. This may due to the fact that we used a circular PWAS in the experimental tests but a square PWAS in FEM simulation.

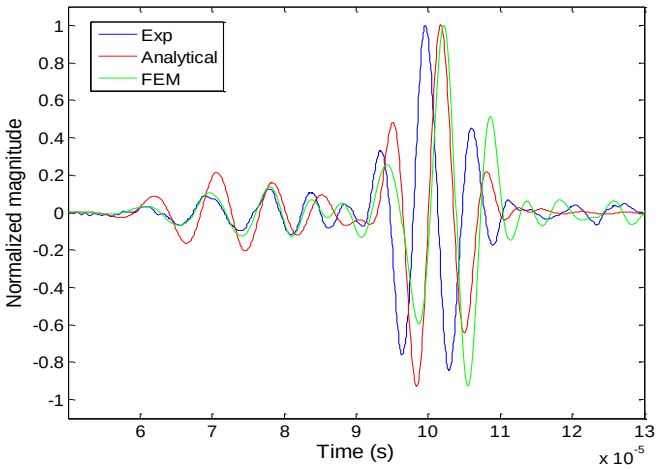

Fig. 7 Experimental, analytical and FEM receive signal by the PWAS P4 in the pristine case

The signal predicted on the pristine plate is compared with the signal modified by the presence of through hole placed between transmitter and receiver. Five holes sizes were considered, 2, 4, 5.9, 7.9, and 9.5 mm. The results for 7.9 mm and 9.5 mm holes are given in Figs. 8(a) and 8(b), respectively. The experimental results are given in Fig. 9. The hole effect on the signal consists of phase shifts and amplitude decreases.

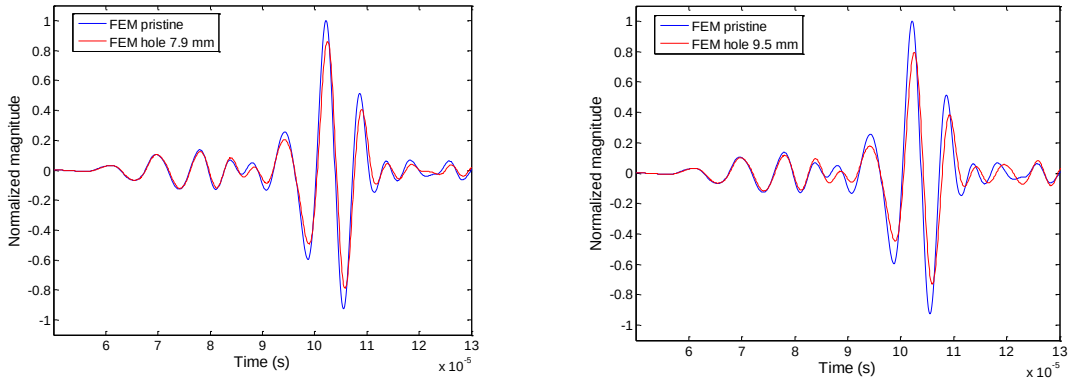

(a) (b)

Fig. 8 FEM comparison between the pristine and the damage signals receive by P4 (a) for a hole damage of 7.9 mm and (b) same for a hole damage of 9.5 mm

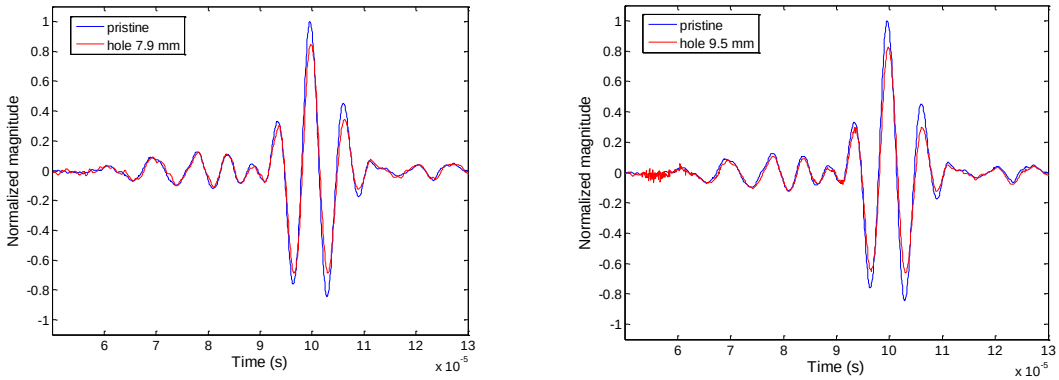

(a) (b)

Fig. 9 Experimental comparison between the pristine and the damage signals receive by P4 (a) for a hole damage of 7.9 mm and (b) same for a hole damage of 9.5 mm

In order to have a system able to evaluate in real time, in situ, the health of the structure in an automatic way, it is necessary to define a damage index (DI). We chose the DI defined by Zhao *et al.* (2007) which gives quite reproducible results and is easy to implement.

$$DI = 1 - \rho \tag{11}$$

In Eq. (11), ρ is the correlation coefficient between two signals defined as

$$\rho = \frac{C_{XY}}{\sigma_X \sigma_Y} \tag{12}$$

where C_{XY} is the covariance of X and Y given by

$$C_{XY} = \sum_{k=1}^{K} (X_k - \mu_x)(Y_k - \mu_y) \tag{13}$$

In Eq. (13), μ the mean of the respective data set and K is the length of the data set. In this case, the data set X is the reference data (baseline) and Y is the new data recorded after a period of service time; σ_X and σ_Y are the standard deviations of x and y, respectively, with their product given by

$$\sigma_X \sigma_Y = \sqrt{\sum_{k=1}^{K} (X_k - \mu_x)^2 (Y_k - \mu_y)^2} \tag{14}$$

This DI was used to detect the hole defect and track its growth in order to compare the experimental and the FEM results. The DI was calculated for different stages of the defect growth. Fig. 10 shows the DI as the diameter of the hole increased from 2 mm through, 4, 6, 7.9 and 9.8 mm. The DI increased with the increase in the defect severity. A very similar slope of the curve is observed between the FEM approach and the experimental results.

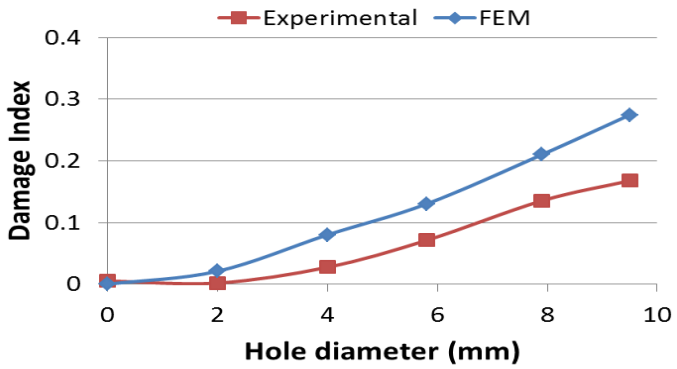

Fig. 10 Comparison of the damage index based on the correlation coefficient between the experimental and the FEM

4.3 Acoustic emission simulation

Simulation of AE was realized using the ABAQUS/implicit software which has multi-physics piezoelectric elements. FEM modeling was used to simulate the elastic wave emitted by the fatigue crack growth. These can be used to compare with the results obtained from the experiment. The dimensions of the plate used for the modeling are shown in Fig. 11. Eight nodes linear piezoelectric brick were used to simulate the PWAS. Implicit solver methods of solution are used.

We explored the use of multi-physics finite element method (MP-FEM) to model the reception of the elastic wave as electric signal recorded at a PWAS receiver (R-PWAS).

The physical properties of the PWAS disks are assumed as

$$[C]=\begin{pmatrix} 97 & 49 & 49 & 0 & 0 & 0 \\ 49 & 97 & 44 & 0 & 0 & 0 \\ 49 & 49 & 84 & 0 & 0 & 0 \\ 0 & 0 & 0 & 24 & 0 & 0 \\ 0 & 0 & 0 & 0 & 22 & 0 \\ 0 & 0 & 0 & 0 & 0 & 22 \end{pmatrix}(\text{GPa}) \tag{15}$$

$$[\varepsilon]=\begin{pmatrix} 947 & 0 & 0 \\ 0 & 947 & 0 \\ 0 & 0 & 605 \end{pmatrix}\times 10^{-8}\left(\text{F.m}^{-1}\right) \tag{16}$$

$$[e]=\begin{pmatrix} 0 & 0 & 0 & 0 & 12.84 & 0 \\ 0 & 0 & 0 & 12.84 & 0 & 0 \\ -8.02 & -8.02 & 18.31 & 0 & 0 & 0 \end{pmatrix}\left(\text{C.m}^{-2}\right) \tag{17}$$

Where $[C]$ is the stiffness matrix, $[\varepsilon]$ is the dielectric matrix and $[e]$ is the piezoelectric matrix. PWAS has a density of $\rho = 7600\ \text{kg.m}^{-3}$, diameter of $7\ \text{mm}$, and thickness of $200\ \mu\text{m}$.

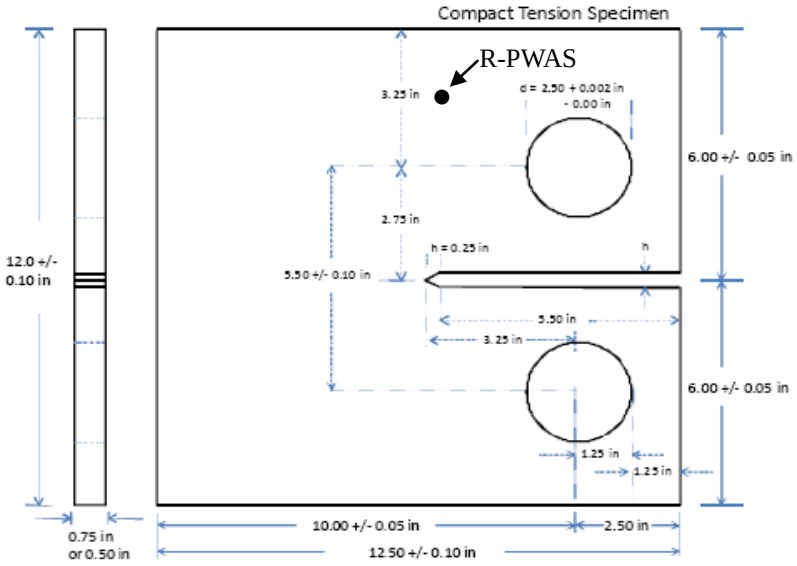

Fig. 11 Plate dimension for the FE model of the thick steel plate. The receiver R-PWAS position was constant

The maximum frequency of interest was chosen at around 500 kHz. For500 kHz, a time interval of 0.1 μs and an element size about 0.5 mm in the steel plate are required to achieve $N = 20$. A step excitation was used as shown in Fig. 12(a). To simulate the energy released by the crack a two-point source force was applied at 0.5 mm from the crack tip as shown in Figs. 12 (b) and 12 (c).

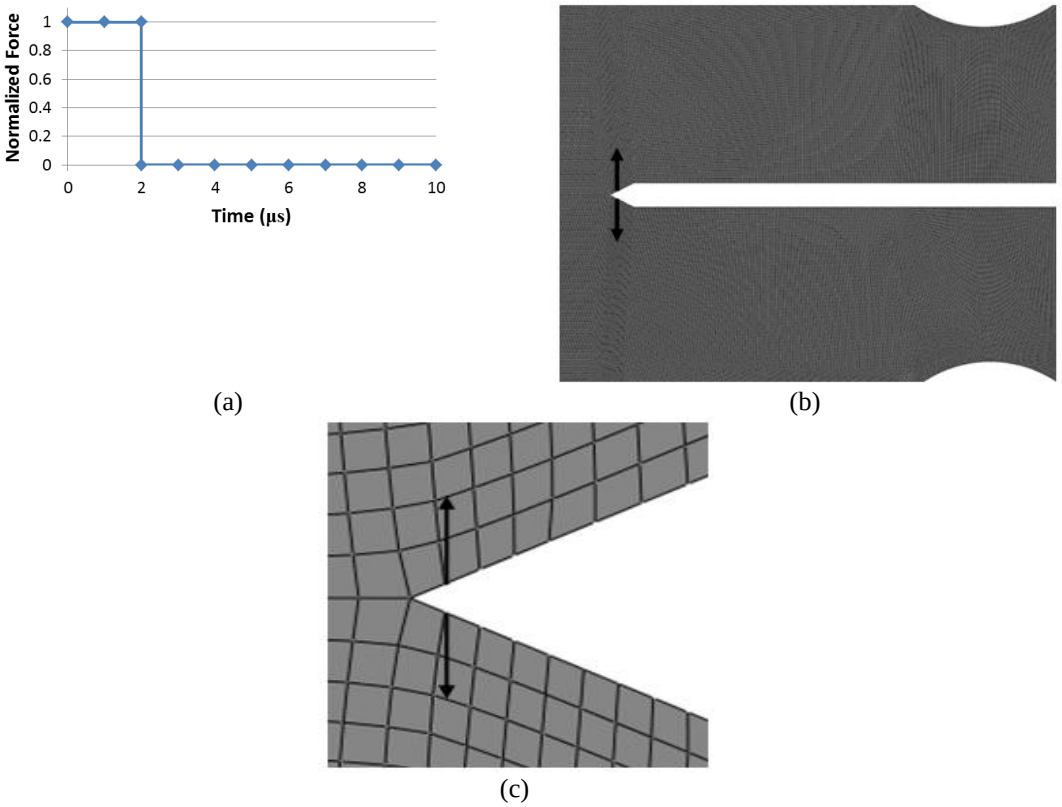

Fig. 12 (a) Source function used: at time zero the force steps up from 0 to a nominal value, 1 and then returns to 0 at 2 μs and (b)-(c) zoom-in and description of the AE simulation source

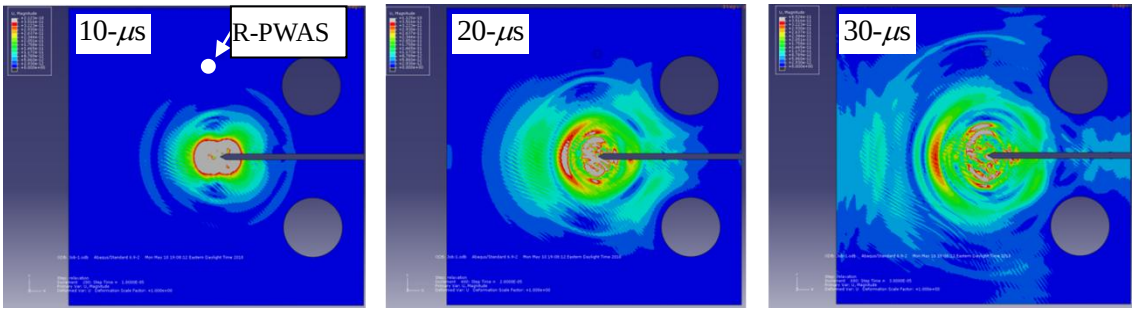

Fig. 13 Multi-physics finite element method (MP-FEM) simulation of guided waves generate by a pair of point forces simulating an acoustic emission by the crack tip

Fig. 13 shows image snapshots of overall displacement amplitude of the guided wave pattern in the plate taken at 10-μs intervals. Multiple guided waves modes are present. At $t = 10\ \mu s$, one sees the waves just starting from crack. By $t = 30\ \mu s$, most of the wave has reflected from the edges of the plate.

The simulated AE signal caused by the crack tip excitation as captured at the R-PWAS is shown in Fig. 14

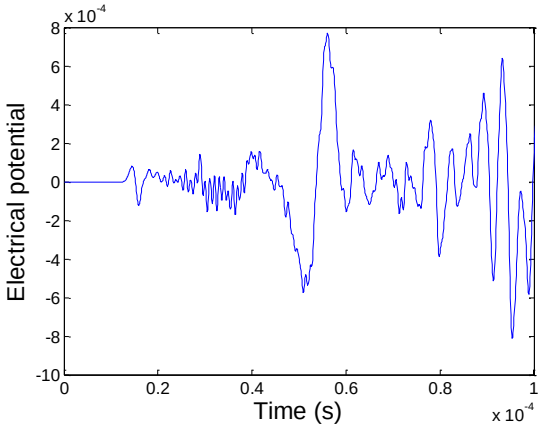

Fig. 14 R-PWAS Output voltage against time

To better understand this signal, we used the discrete wavelet transform (DWT). The DWT of a time signal $s(t)$ is the result of the convolution product between the signal $s(t)$ and a family of "daughter wavelets" $\gamma_{m.k}(t)$, (Morlet *et al. 1*982) i.e.

$$DWT_{m,k} = \int_0^{\infty} s(t)\gamma_{m,k}(t)dt \tag{18}$$

The main particularity of the DWT is that the result obtained with each daughter wavelet corresponds to the time behavior of the signal in a frequency band corresponding to dilatation factor *m*. Each response is called the decomposition level. A number of different bases have been proposed to construct a family of wavelets. A good solution for analysis and decomposition can be obtained with the Daubechies wavelet (Daubechies 1992). The application of discrete wavelet analysis to the acquired AE signals resulted in its decomposition into six different levels. Each level represents a specific frequency range, and the frequency range increases with increasing wavelet level. The decomposed AE signals in level 1 to 6 are shown in Fig. 15.

The Fourier spectrum of the Fig. 15 signals is shown in Fig. 16. The frequency spectra for DWT levels 1 through 6 are centered at about 58 kHz, 88 kHz, 186 kHz, 518 kHz, 1 MHz and 1.48 MHz, respectively. We also investigated the effect of the frequency on the excited wave amplitude. At frequencies 58 kHz and 88 kHz (Daubechies wavelet levels 1 and 2), two modes exist (Fig. 17(a)), the fundamental symmetric mode (S0) and the fundamental anti-symmetric mode (A0). As shown in Fig. 17(b), the amplitude of the A0 mode is higher than the S0 mode, and its travel speed is slower (Fig 17(a)). At 186 kHz (Daubechies wavelet level 3), three modes exist, S0, A0, and A1; the amplitude of the A_0 and A_1 modes are much higher than the S0 mode which is close to zero. But

at this frequency, the A0 and the A1 modes are faster than the S0 mode. At 518 kHz (Daubechies wavelet level 4), seven modes exist, S0, S1, S2, A0, A1, A2 and A3. So at this frequency and for the higher frequency (1 MHz and 1.48 MHz) we cannot distinguish the different wave packets and the signal processing is very complicated. We can also note in Fig. 16 that the amplitude is distributed such that it is the highest in level 1 and lowest in level 6.

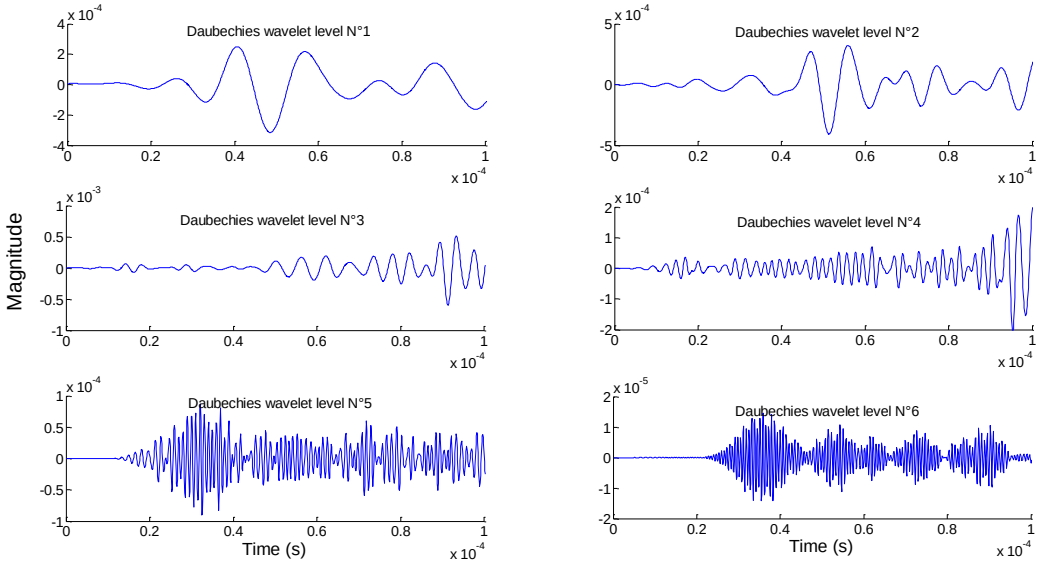

Fig. 15 Discrete wavelet transform of the simulated signal received by the PWAS

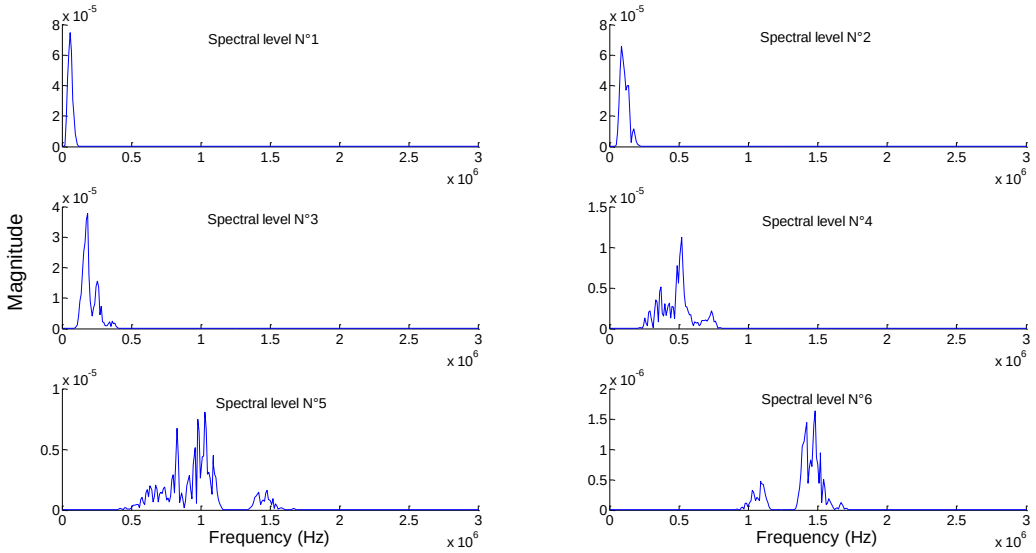

Fig. 16 Frequency spectra for the different wavelet level

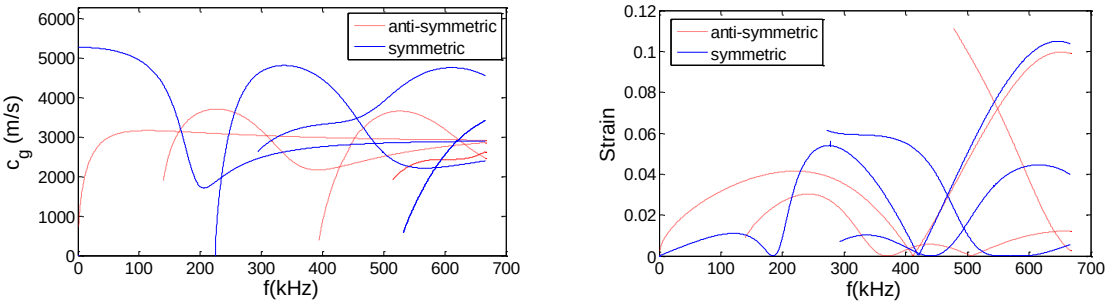

Fig. 17 Theoretical prediction (a) the group velocity of the symmetric and anti-symmetric modes and (b) the frequency tuning

Fig. 18 shows the Continuous Wavelet Transform (CWT) magnitude as a function of frequency versus time. The CWT were calculated with AGU-Vallen Wavelet, a freeware software program (Vallen-System 2001). This program has a Gabor function as the "mother" wavelet. The Fig. 18 shows the four lowest modes (S0, A0, S1 and A1) superposed on the CWT plot. This superposition is facilitated by an option that converts the group velocity scale to a time scale using the known propagation distance. The color scale in the Fig. 18 is a linear scale with red representating the highest magnitude region of the CWT and pink the smallest or zero-magnitude region. Clearly, Fig. 18 shows the presence of AE signal energy in portions of the four modes. The CWT shows how the signal energy is distributed as a function of frequency, time (or group velocity), and mode. Fig. 18 shows that the AE source has the greatest concentration (most red color) of energy is the fundamental anti-symmetric mode A0 in a frequency range of 50 to 120 kHz. Another large amplitude region of the CWT is the part of the fundamental symetric mode S0 and the anti-symmetric mode A1 in a frequency range 220 to 270 kHz. This demonstrates that the AE signal energy is not uniformly distributed between the modes; it is also not uniformly distributed as a function of frequency along each of the dominant modes.

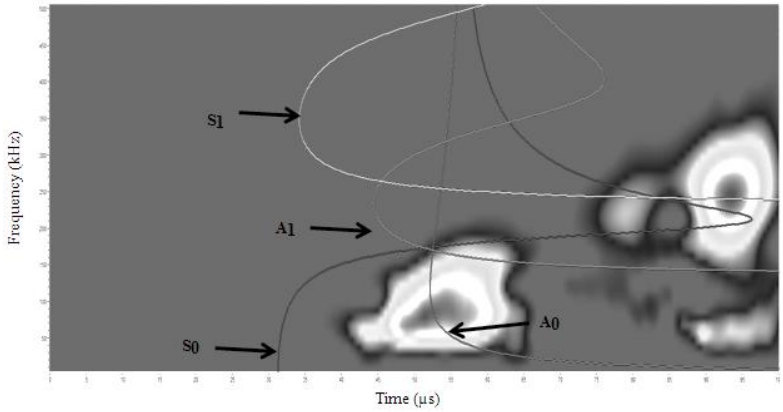

Fig. 18 Superimposed symmetric mode and anti-symmetric modes after converting group velocity to time based on the propagation distance

The above discussion proves that the waveforms features (duration time, amplitude, time-frequency spectrum) are useful to illustrate the characteristics of AE signal and distinguish the different AE signals associated with various possible failure modes in the specimens.

5. Experimentals results

5.1 PWAS AE detection tests on I-beam

The use of PWAS transducers as AE sensors were first investigated by comparing with a conventional AE transducer PAC R15I on an 8-mm thick steel I-beam in a laboratory environment. The two sensors were placed face to face on the opposite surfaces of an I-beam (Fig. 19). Pencil lead breaks were made 10-mm away from the PWAS center to simulate the acoustic emission source. The recorded data were compared to investigate relative performance of these sensors. As seen in Fig. 19, PWAS and R15I produced very similar signals. We also found that the amplitudes follow the predicted decay proportional to the inverse of the square root of the distance away from the sensor position, as shown in Fig. 20.

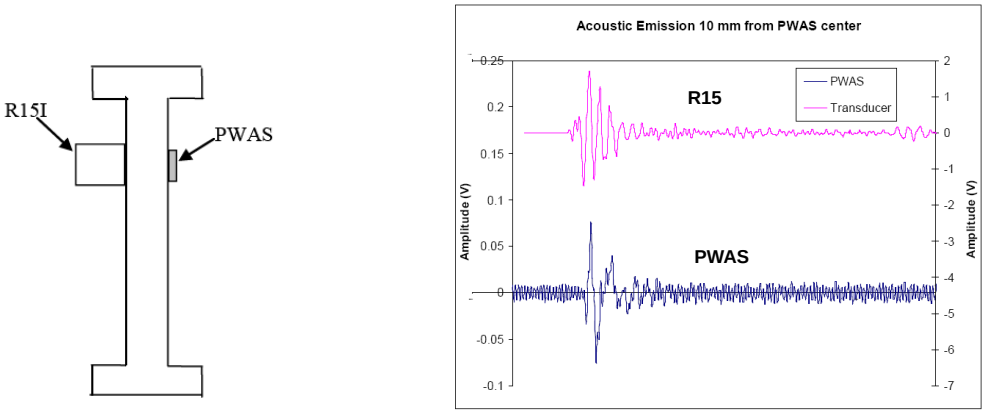

Fig. 19 Comparison of PWAS AE sensor and R15I during a pencil break AE test on an 8 mm steel l-beam

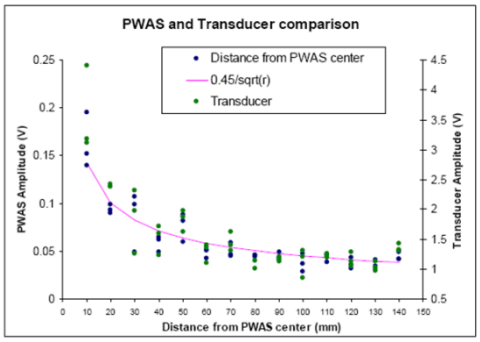

Fig. 20 Amplitude curves of PWAS and R15I on an 8 mm steel I-beam

5.2 Crack detection on compact tension specimens

Compact Tension (CT) specimens ASTM E647 made of structural steel A572 grade 50 were used in this study (Fig. 22). The effective width of the CT specimen as defined in ASTM E647 is 9.5 inches. The thickness and notch length are 0.5 inch and 3.25 inches, respectively. The cyclic tension loads were applied to the specimen using servo hydraulic mechanical testing machine MTS 810. First, a static load was applied to the specimen. Then the tension load was applied with a minimum of 0.5 kN and a maximum of 50 kN. Fatigue tests were conducted under load-controlled mode with frequency of 1 HZ. The cracks were monitored optically with a high resolution recording microscope. Four PWAS were installed on the specimen as shown in Fig. 22(a). A combined passive AE and active guided wave sensing were conducted to detect and quantify the crack growth. In addition, five R15I were mounted on the opposite side of the specimen to compare the AE signals received from the crack by these two different sensors.

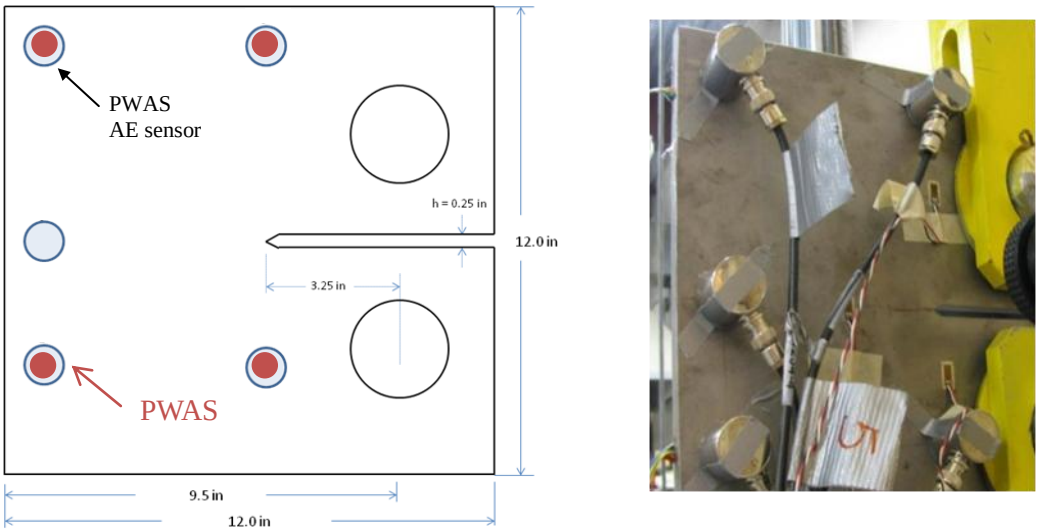

Fig. 21 PWAS AE CT testing: (a) Specimen Layout, (b) photo of the specimen and (c) test setup layout

5.2.1 Passive AE sensing

To improve the signal-to-noise ratio, PAC 2-4-6 voltage preamplifier with built-in 100-1200 kHz bandpass filter were used with PWAS providing 40 dB amplifying factor. AE data was recorded and displayed through a 16-channel PAC Sensor Highway II-Remote Asset Integrity Monitor. The time driven rate was set at 100 ms, which permitted 10 data points to be collected in a load cycle for various parameters such as strain and load. The fixed threshold (trigger point) of each acoustic emission channel was 45 dB. Band pass analogue filter was set at 100 kHz to 1 MHz. For comparison, five R15I AE transducers were mounted on the opposite side of the specimen to collect AE as well.

A lead break test was performed near the tip of the crack to test whether the transducers are working properly. The comparison of crack localization analyzed by PAC AEwin software between PWAS AE sensor and R15I is shown in Fig. 22 . 1171 AE events were detected with R15I before the final failure, while 54 were detected by PWAS. From Fig. 22 (b), it can be seen that PWAS localization is closer and concentrated around the crack tip compared with the R15I detection in Fig. 22(a). This might be caused by the higher sensitivity of R15I, which detected both AE signals and noises. We could reduce these false alarms by increasing the threshold.

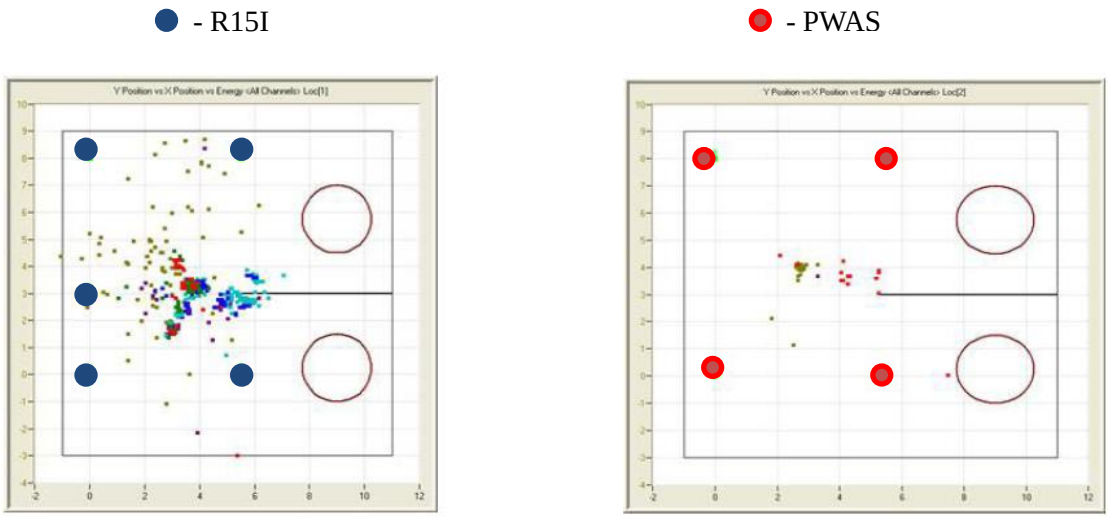

(a) (b)

Fig. 22 Comparison of crack localization in CT test on 12.7 mm steel specimen, (a) crack localization by R15I and (b) crack localization by PWAS (Yu *et al.* 2010)

5.2.2 Active guided wave sensing

Aside from the passive AE sensing, the four PWAS have also been used in active mode for guided wave interrogation actuation and reception to detect and quantify the length of the crack (Fig. 23).

We used the DI definition described in section 4.2 Eqs. (11)-(14) to track the evolution of DI against the crack growth for path P0 to P1 (P0 being the transmitter and P1 the receiver). Fig. 24 (a)

shows that the DI increased with crack growth when the crack is placed in the direct wave propagation path like P0 to P1. In this case the detection is possible when the crack dimension is greater than 10 mm. For the other paths, the DI also changes with crack growth, but to a lesser extent (Fig. 24(b)). For crack lengths less than 20 mm, the DI values are 'noisy' and do not present a definite indication of damage. For crack lenghts greater than 20 mm, the DI values seem to increase monotonically, indicating that 20 mm might be the detection threshold for the paths not directly traversing the crack path.

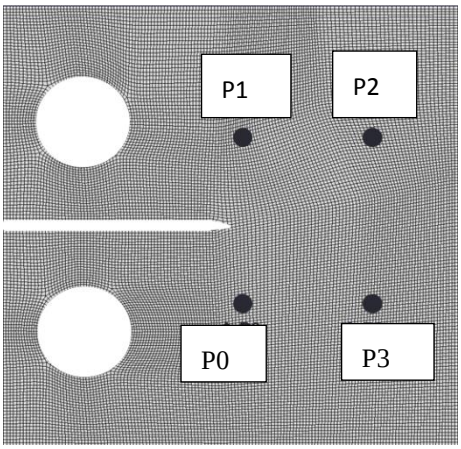

Fig. 23 Active PWAS layout for the excitation and the reception of guided waves

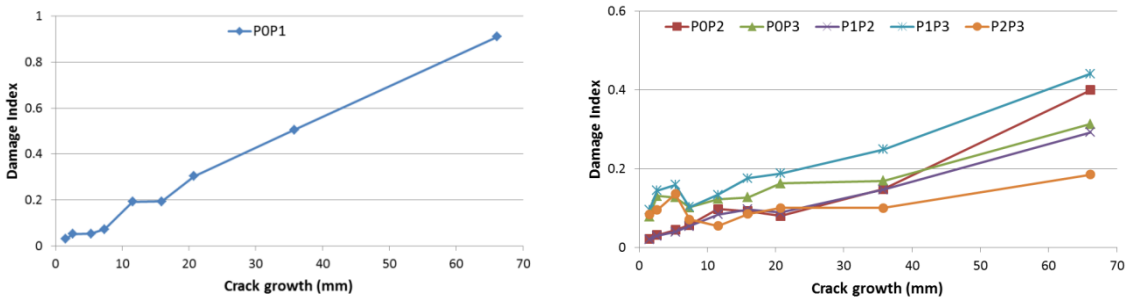

(a) (b)

Fig. 24 Damage index based on the correlation coefficient, (a) for the path P0 to P1 and (b) for the other paths

6. Conclusions

This paper has presented numerical and experimental results on the use of guided waves for SHM of crack growth during a fatigue test in a thick steel plate used for civil engineering application. The capability of embedded PWAS to perform in situ NDE has been explored. Numerical simulation and experimental tests have been used to prove that PWAS can perform both

passive SHM using AE method and active SHM using guided wave pitch-catch method.

FEM codes were used to simulate the transmission and reception of guided waves in a 12.7-mm plate and their diffraction by a through hole. This simulation obtained a good match compared to the experimental results and showed that is possible to detect the scattering wave from hole in a thick plate.

AE simulation has been conducted with the MP-FEM approach in a 12.7-mm plate in the shape of the CT fracture mechanics specimen. The AE event was simulated as a pulse of defined duration and amplitude. The simulated electrical signal was measured at a receiver PWAS using the MP-FEM capability with the piezoelectric element. Daubechies wavelet transforms and their FFT frequencies was used to process the active signal in order to define and separated the different modes that composed the AE signal.

Experimental tests were performed with PWAS transducers acting as passive receivers of AE signals. The 8-mm thick flange of an I-beam was instrumented on one side with PWAS transducers and on the other side with conventional AE transducers R15I for comparison. An AE source was simulated using 0.5-mm pencil lead breaks; the PWAS transducers were able to pick up AE signals of adequate strength. Subsequently, PWAS transducers and R15I sensors are applied to a 12.7-mm thick CT specimen subjected to accelerated fatigue testing. Though both sensors were able to detect the AE sources, we found that PWAS localization is closer and more concentrated around the actual crack tip compared with the R15I detection. Active sensing in pitch catch mode was also adopted using the same PWAS transducers installed on the CT specimen. Damage indexes were calculated and correlated with physical crack growth as optically measured.

In this paper, we have also shown the contribution of the FEM simulation to the better understanding of the wave propagation in thick steel plates. This gives an added advantage when it is combined with PWAS to simulate the full propagation and detection process. The modeling process provides the potential for large cost savings and a better understanding of complex SHM problems. In the case of AE signals, the process of generation, propagation and detection is very complex. In the future, more works needs to be done on (a) calibrating the MP-FEM modeling of guided wave for accurate representation of physical phenomenon; (b) simulate the real energy release of crack growth using XFEM or VCCT model; (c) better understand the multi-modal guided wave propagation in thick steel plates and identify more effective wave-tuning methods and signal processing algorithm for damage identification and localization.

Acknowledgements

This work is performed under the support of the U.S. Department of commerce, National Institute of standards and Technology (NIST), Technology Innovation Program, Cooperative Agreement Number #70NANB9H9007.

References

Achenbach, J.D. (1973), *Wave propagation in Elastic Solids*: North-Holland series, in Applied Mathematics and Mechanics.

Alleyne, D.N. and Cawley, P. (1992), "The interaction of Lamb waves with defects", *IEEE T. Ultrason. Ferr.*, **39**(3), 381-397.

Castaings, M. (2002), *Contrôle et évaluation non destructifs de matériaux par ondes ultrasonores guidées*, Ph.D. thesis, Université de Bordeaux 1.

Daubechies, I. (1992), *Ten lectures on wavelets*, Philadelphia, PA: Society for Industrial and Applied Mathematics, ISBN-10: 0898712742

Dietzhausen, H., Dong, M. and Schmauder, S. (1998), "Numerical simulation of acoustic emisssion in fiber reinforced polymer", *Comput. Mater. Sci*., **13**, 23-30.

Dieulesaint, E. and Royer, D. (1996), *Ondes élastiques dans les solides- Tome 1: Propagation libre et guidée*, Paris: Masson.

Frankenstein, B., Hentschel, D. and Schubert, F. (2006), *Monitoring network for SHM in avionic applications*, ECNDT - Th1.7.3.

Giurgiutiu, V. (2005), "Tuned Lamb-wave excitation and detection with piezoelectric wafer active sensors for structural health monitoring", *J. Intell. Mater. Syst. Struct*., **16**(4), 291-306.

Giurgiutiu, V. (2008), *Structural health monitoring with piezoelectric wafer active sensors*, Elsevier Academic Press, 760, ISBN 978-0120887606,

Giurgiutiu, V., Gresil, M., Lin, B., Cuc, A., Shen, Y. and Roman, C. (2012), "Predictive modeling of piezoelectric wafer active sensors interaction with high-frequency structural waves and vibration", *Acta Mech*., doi: 10.1007/s00707-012-0633-0.

Gorman, M.R. and Proser, W.H. (1991), "AE source by plate analysis", *J. Acoustic Emission*, **9**(4), 238-288.

Graff, K.F. (1975), *Wave motion in elastic solids*, Oxford University Press:London, ISBN-10:0486667456.

Grahn, T. (2003), "Lamb wave scattering from a circular partly through-thickness hole in a plate", *Wave Motion*, **37**(1), 63-80.

Gresil, M., Lin, B., Shen, Y. and Giurgiutiu, V. (2011a), "Predictive modeling of space structures for SHM with PWAS transducers", *Proceedings of the ASME Conference* (54723), 525-534.

Gresil, M., Shen, Y. and Giurgiutiu, V. (2011b), "Predictive modeling of ultrasonics SHM with PWAS transducers", *Proceedings of the 8th International Workshop on Structural Health Monitoring*, San-Francisco, CA, USA.

Gresil, M., Shen, Y. and Giurgiutiu, V. (2012), "Benchmark problems for predictive FEM simulation of 1-D and 2-D guided wave for structural health monitoring with piezoelectric wafer active sensors", *Proceedings of the Review of Progress in Quantative Nondestructive Evaluation* AIP Conf., **1430**(1), 1835-1842, doi: 10.1063/1.4716434.

Greve, D.W., Zheng, P. and Oppenheim, I.J. (2008), "The transition from Lamb waves to longitudinal waves in plates", *Smart Mater. Struct*., **17**(3), 035029.

Grondel, S., Assaad, J., Delebarre, C., Blanquet, P. and Moulin, E. (1999), "The propagation of lamb waves in multilayered plates: phase-velocity measurement", *Meas. Sci. Technol.*, **10**(5), 348-353.

Grondel, S., Delebarre, C., Assaad, J., Dupuis, J.P. and Reithler, L. (2002), "Fatigue crack monitoring of riveted aluminium strap joints by Lamb wave analysis and acoustic emission measurement techniques", *NDT & E Int*., **35**(3), 137-146.

Han, S. (2007), *Finite element analysis of lamb waves acting within a thin aluminum plate*, Thesis, Department of Aeronautical and Astronautical Engineering, Air Force Institute of Technology.

Harker, A.H. (1987), *Elastic waves in solids*. Bristol: British gas/Adam Hilger.

Hill, R., Forsyth, S.A. and Macey, P. (2004), "Finite element modeling of ultrasound, with reference to transducers and AE waves", *Ultrasonics*, **42**(1-9), 253-258.

Lamb, H. (1917), "On waves in an elastic plate", *P. Roy. Soc. London. Series A*, **93**(648), 114-128.

Lee, C.K., Scholey, J.J., Wilcox, P.D., Wisnom, M.R., Friswell, M.I. and Drinkwater, B.W. (2006), "Guided wave acoustic emission from fatigue crack growth in aluminum plate", *Adv. Mater. Res*., **13**, 23-28.

Lemistre, M. and Balageas, D. (2001), "Structural health monitoring system based on diffracted Lamb wave analysis by multi-resolution processing", *Smart Mater. Struct*., **10**(3), 504-511.

Liu, W. and Giurgiutiu, V. (2007) "Finite element simulation of piezoelectric wafer active sensors for structural health monitoring with coupled-field elements", *Proceedings of the ASME International Mechanical Engineering Congress and Exposition*, IMECE 2007-43570, 715-726.

Lowe, M.J.S. and Diligent, O. (2002), "Low-frequency reflection characteristics of the S0 Lamb wave from

a rectangular notch in plate", *J. Acoust. Soc. Am*., **111**(1), 64-74.
Lu, Y., Ye, L., Su, Z. and Yang, C. (2008), "Quantitative assessment of through-thickness crack size based on Lamb wave scattering in aluminum plates", *NDT & E Int.*, **41**(1), 59-68.
Mal, A. K. and Chang, Z. (1999), "Scattering of lamb wave from a rivet hole with edge cracks", *Mech. Mater*., **31**, 197-204.
Moder, F. and Jacobs, L.J. (1998), "Application of finite element methods to study transient wave propagation in elastic waves guides", *Rev. Prog. Quantitative NDE*, **17**, 161-167.
Morlet, J., Arens, G., Fourgeau, I. and Giard, D. (1982), "Wave Propagation the Mixing Layer: Application of the 2-D Arc Wavelet Transform", Journal of and Sampling Theory", *Geophysics*, **47**, 203-236.
Rose, J.L. (1999), *Ultrasonic waves in solid media*, Cambridge University: Cambridge University Press.
Santoni-Bottai, G., Yu, L., Xu, B. and Giurgiutiu, V. (2007), "Lamb wave mode tuning of piezoelectric wafer active sensors for structural health monitoring", *J. Vib. Acoust*., **129**(6), 752-762.
Scruby, C.B., Baldwin, G.R. and Stacey, K.A. (1985), "Characterization of fatigue crack extension by quantitative acoustic emission", *Int. J. Fracture*, **28**, 201-222.
Titry, C., Terrien, N. and Lepoutre, F. (2004), D*etection de la corrosion cachée dans les structures aéronautiques en aluminium* Colloque Interdisciplinaire en Instrumentation (CII), Cachan, France.
Vallen-System, GmbH. (2001), http://www.vallen.de/wavelet/index.html, Munich, Germany.
Viktorov, I.A. (1967), *Rayleigh and lamb waves - physical theory and application*, New York Plenum Press.
Wang, X., Lu, Y. and Tang, J. (2008), "Damage detection using piezoelectric transducers and the Lamb wave approach: I. System analysis", *Smart Mater. Struct*., **17**(2), 025033.
Wilcox, P., Lowe, M. and Cawley, P. (2001), "The effect of dispersion on long-range inspection using ultrasonic guided waves", *NDT & E Int.*, **34**(1), 1-9.
Yang, Y. and Hu, Y. (2008), "Electromechanical impedance modeling of PZT transducers for health monitoring of cylindrical shell structures", *Smart Mater. Struct*., **17**(1), 015005.
Yu, L., Giurgiutiu, V., Ziehl, P., Ozevin, D. and Pollock, P. (2010), "Steel bridges fatigue crack detection with piezoelectric wafer active sensors", *Proceedings of the SPIE conference on Sensors and Smart Structures Technologies for Civil, Mechanical, and Aerospace Systems*.
Zak, A., Krawczuk, M. and Ostachowicz, W. (2006), "Propagation of in-plane waves in an isotropic panel with a crack", *Finite Elem. Anal. Des*., **42**(11), 929-941.
Zhao, X., Gao, H., Zhang, G., Ayhan, B., Yan, F., Kwan, C. and Rose, J.L. (2007), "Active health monitoring of an aircraft wing with embedded piezoelectric sensor/actuator network: I. Defect detection, localization and growth monitoring", *Smart Mater. Struct*., **16**(4), 1208-1217.

CC